Analysis of the Structural Determinants Underlying Discrimination between Substrate and Solvent in β-Phosphoglucomutase Catalysis[†,‡]

Jianying Dai,[§] Lorenzo Finci,[||] Chunchun Zhang,[§] Sushmita Lahiri,[||] Guofeng Zhang,[§] Ezra Peisach,[||] Karen N. Allen,*[,||,⊥] and Debra Dunaway-Mariano*[,§]

Department of Chemistry, University of New Mexico, Albuquerque, New Mexico 87131, and Department of Physiology and Biophysics, Boston University School of Medicine, Boston, Massachusetts 02118-2394

Received August 31, 2008; Revised Manuscript Received January 17, 2009

ABSTRACT: The β-phosphoglucomutase (β-PGM) of the haloacid dehalogenase enzyme superfamily (HADSF) catalyzes the conversion of β-glucose 1-phosphate (βG1P) to glucose 6-phosphate (G6P) using Asp8 of the core domain active site to mediate phosphoryl transfer from β-glucose 1,6-(bis)phosphate (βG1,6bisP) to βG1P. Herein, we explore the mechanism by which hydrolysis of the β-PGM phospho-Asp8 is avoided during the time that the active site must remain open to solvent to allow the exchange of the bound product G6P with the substrate βG1P. On the basis of structural information, a model of catalysis is proposed in which the general acid/base (Asp10) side chain moves from a position where it forms a hydrogen bond to the Thr16-Ala17 portion of the domain−domain linker to a functional position where it forms a hydrogen bond to the substrate leaving group O and a His20-Lys76 pair of the cap domain. This repositioning of the general acid/base within the core domain active site is coordinated with substrate-induced closure of the cap domain over the core domain. The model predicts that Asp10 is required for general acid/base catalysis and for stabilization of the enzyme in the cap-closed conformation. It also predicts that hinge residue Thr16 plays a key role in productive domain−domain association, that hydrogen bond interaction with the Thr16 backbone amide NH group is required to prevent phospho-Asp8 hydrolysis in the cap-open conformation, and that the His20-Lys76 pair plays an important role in substrate-induced cap closure. The model is examined via kinetic analyses of Asp10, Thr16, His20, and Lys76 site-directed mutants. Replacement of Asp10 with Ala, Ser, Cys, Asn, or Glu resulted in no observable activity. The kinetic consequences of the replacement of linker residue Thr16 with Pro include a reduced rate of Asp8 phosphorylation by βG1,6bisP, a reduced rate of cycling of the phosphorylated enzyme to convert βG1P to G6P, and an enhanced rate of phosphoryl transfer from phospho-Asp8 to water. The X-ray crystal structure of the T16P mutant at 2.7 Å resolution provides a snapshot of the enzyme in an unnatural cap-open conformation where the Asp10 side chain is located in the core domain active site. The His20 and Lys76 site-directed mutants exhibit reduced activity in catalysis of the Asp8-mediated phosphoryl transfer between βG1,6bisP and βG1P but no reduction in the rate of phospho-Asp8 hydrolysis. Taken together, the results support a substrate induced-fit model of catalysis in which βG1P binding to the core domain facilitates recruitment of the general acid/base Asp10 to the catalytic site and induces cap closure.

Phosphomutases catalyze the movement of a phosphoryl group from one position in a phosphorylated metabolite to another as needed to initiate or to continue a catabolic pathway [examples include α-phosphoglucomutase (*1*) and phosphoglycerate mutase (*2*) of the glycolysis pathway and β-phosphoglucomutase (*3*) of the trehalose/maltose degradation pathways] or to form the precursor to a biosynthetic pathway [examples include α-phosphomannomutase (*4*), α-phosphoglucoseamine mutase (*5, 6*), and α-phosphoglucomutase (*7*) which function in the biosynthesis of membrane-bound, cell wall, or capsular glycans]. The mechanisms by which phosphomutases orchestrate the transfer of the phosphoryl group between substrate positions have intrigued scientists for decades (*5, 8*−*10*).

Phosphomutases have evolved within several different enzyme superfamilies, including the histidine phosphatase (*11*), alkaline phosphatase (*12*), haloacid dehalogenase (HAD) (*13*), and phosphohexomutase superfamilies (*14*), yet they share a common catalytic strategy, the use of an active site nucleophile (His, Ser, Asp, and Ser, respectively) to mediate the transfer of the phosphoryl group. Catalysis in

[†] This work was supported by NIH Grant GM61099 to K.N.A. and D.D.-M. Financial support for X12C at Brookhaven National Laboratory comes principally from the Offices of Biological and Environmental Research and of Basic Energy Sciences of the U.S. Department of Energy and the National Center for Research Resources of the National Institutes of Health.

[‡] Coordinates for the T16P mutant of β-phosphoglucomutase have been deposited in the Protein Data Bank as entry 3FM9.

* To whom correspondence should be addressed. D.D.-M.: e-mail, dd39@unm.edu; phone, (505) 277-3383; fax, (505) 277-2609. K.N.A.: phone, (617) 358-5544; fax, (617) 358-5554; e-mail, drkallen@bu.edu.

[§] University of New Mexico.

[||] Boston University School of Medicine.

[⊥] Present address: Department of Chemistry, Boston University, Boston, MA 02215.

10.1021/bi801653r CCC: $40.75
Published on Web 01/20/2009

the phosphomutases of the histidine phosphatase, HAD, and phosphohexomutase superfamilies proceeds via a bisphosphate intermediate (*11, 15*−*17*), whereas catalysis in the phosphoglycerate mutase of the alkaline phosphatase family proceeds via a glycerate intermediate. Each mutase requires that the intermediate reorient in the active site. The glycerate reorients in the active site of the phosphorylated phosphoglycerate mutase by flipping (*18*). The reorientation of the bisphosphate intermediate in the spacious active site of the phosphohexomutase superfamily mutases also occurs by flipping, whereas the confined active sites of the HAD superfamily (HADSF) mutases require that the intermediate must dissociate into solvent and then bind in the opposite orientation (*15*−*17*).

The topic of this paper is the β-phosphoglucomutase (β-PGM)[1] of the HADSF. The HADSF is comprised mostly of phosphohydrolases (phosphatases and ATPases), which conserve a Rossmann fold core domain (Figure 1) (*19*). The core domain catalytic scaffold consists of four peptide segments or loops on which the Mg^{2+} cofactor-binding residues and the catalytic residues, which constitute the core domain active site, are located (Figure 1). The conserved Asp nucleophile (Asp8 in β-PGM) of loop 1 mediates phosphoryl transfer in all HADSF phosphotransferases. HADSF phosphatases and mutases conserve a second Asp (Asp10 in β-PGM) located two positions downstream of the Asp nucleophile to participate in general acid/base catalysis (*20*).

In most HADSF members, the core domain is linked to a cap domain that, when associated with the core domain, aids in active site desolvation and assists in binding the substrate-leaving group (*21*−*24*). The type C1 cap domain (*13*) of β-PGM (Figure 2A) works in concert with the core domain to catalyze phosphoryl transfer to and from the C(6)O and C(1)O positions of β-glucose 1-phosphate (βG1P) and β-glucose 1,6-bisphosphate (βG1,6bisP) (*10, 15, 25*). The catalytic cycle (Figure 2B) consists of the integration of ligand binding and dissociation to and from the active site of the cap-open conformer and catalysis of phosphoryl transfer to and from the active site Asp8 nucleophile of the cap-closed conformer. β-PGM is distinguished from the HADSF phosphatases and ATPases by the selection of βG1P versus water to accept the phosphoryl group from phospho-Asp8. The mechanism by which β-PGM makes the distinction between substrate and solvent as the phosphoryl group acceptor is the focus of this work.

The β-PGM cap-open and cap-closed conformations can be compared by examination of the X-ray structures of the phosphorylated β-PGM(Mg^{2+}) complex (*3*) and the β-PGM(Mg^{2+})(βG1,6bisP) complex (*25*), respectively. The β-PGM cap and core domains are connected by two parallel, solvated peptide segments (Figure 1B). The cap domain rotates by 26° relative to the core domain via a change in the backbone ϕ and ψ angles of linker hinge residues Thr14, Asp15, Thr16, and Ala17 to open and close the entrance to the core domain active site. In the cap-open conformer, the Asp10 side chain carboxylate group is pinned into a position outside the active site via hydrogen bond formation with the backbone amide NH groups of hinge residues Thr16 and Ala17 (Figure 3). In the cap-closed conformer, the Asp10 side chain carboxylic acid group is positioned in the core domain active site, where it engages in a hydrogen bond network that includes the βG1,6bisP C(1)O group and a His20-Lys76 cap domain pair. Thus, the two β-PGM structures show that the Asp10 side chain alternates (via a 136° rotation about the Cα−Cβ bond) between the linker site in the cap-open conformation and the catalytic site in the cap-closed conformation.

Herein, we propose and evaluate a substrate induced-fit model for the mechanism by which phosphoryl transfer from β-PGM phospho-Asp8 to water is avoided in the presence

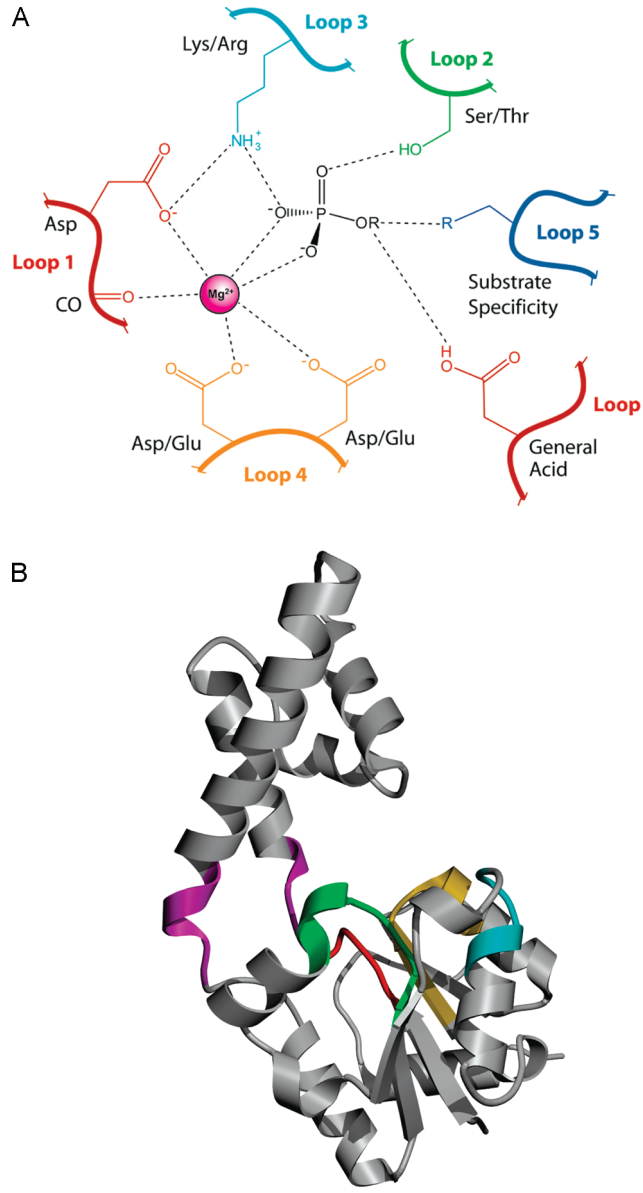

FIGURE 1: HASDF phosphotransferase catalytic scaffold. The coloring scheme used to identify the four loops is as follows: red for loop 1, green for loop 2, cyan for loop 3, gold for loop 4, and magenta for linker regions. (A) Schematic of the interactions that occur between a generic phosphoester substrate and the conserved residues of the scaffold. (B) Position of the conserved catalytic loops on the core Rossmann domain of β-phosphoglucomutase.

[1] Abbreviations: α-PGM, α-phosphoglucomutase; α-PGM/PMM, dual-specificity α-phosphoglucomutase/α-phosphomannomutase; β-PGM, β-phosphoglucomutase; E, β-PGM−Mg^{2+}; E−P, phospho-β-PGM−Mg^{2+}; βG1P, β-D-glucose 1-phosphate; βG1,6bisP, β-D-glucose 1,6-(bis)phosphate; αG1P, α-D-glucose 1-phosphate; αG1,6bisP, α-D-glucose 1,6-(bis)phosphate; PDB, Protein Data Bank; PEP, phosphoenolpyruvate; SA, specific activity.

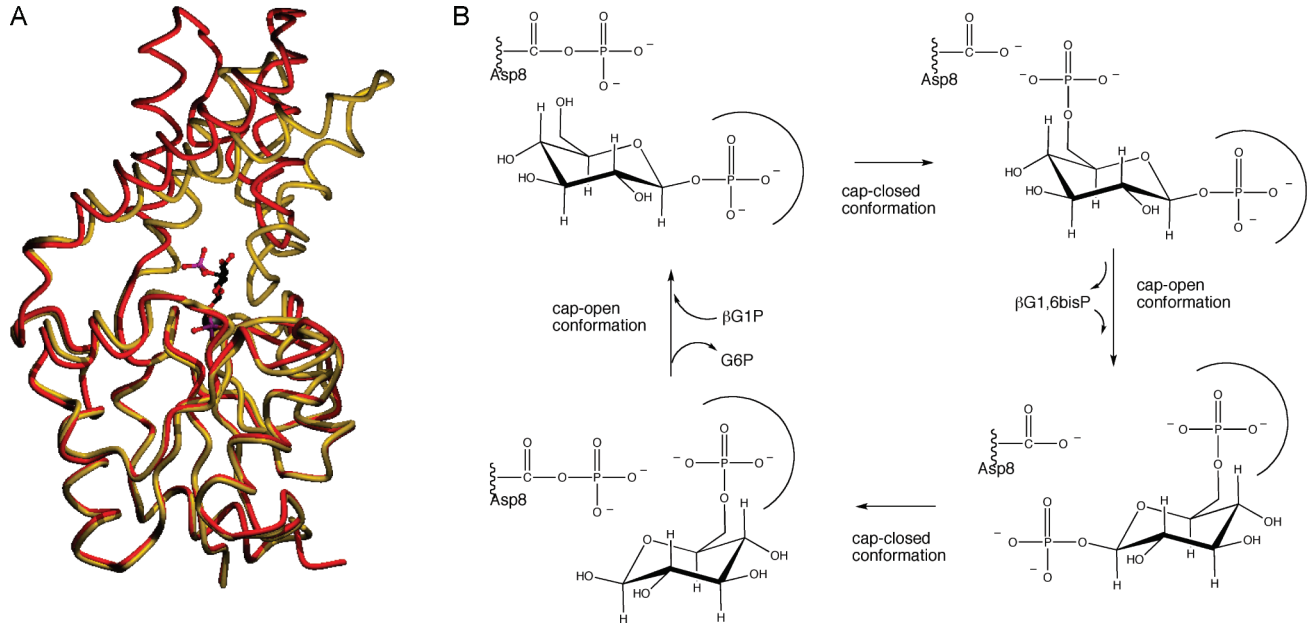

FIGURE 2: Structural and catalytic cycling in β-PGM. (A) Overlay of the backbone Cα atom positions of the unliganded [PDB entry 1LVH (red)] and βG1,6bisP complex [PDB entry 1O08 (gold)] forms with βG1,6bisP shown in ball-and-stick format and the Mg^{2+} cofactor as a gray sphere. (B) Schematic depiction of the catalytic cycle.

of βG1P. The model assumes that Asp10 acts in general acid/base catalysis to stabilize the enzyme in the catalytically active cap-closed conformation. Site-directed mutagenesis and kinetic analyses of mutant enzymes were used to demonstrate that Asp10 is indeed essential to β-PGM catalysis. The model also predicts that the linker plays two key roles in catalysis: (1) to pin the Asp10 side chain outside of the active site in the unliganded, phosphorylated enzyme and thus prevent general base-catalyzed phosphoryl transfer to water and (2) to allow, via main chain conformational change, the coordinated movement of the cap and core domains that occurs during catalytic cycling. Thr116 was identified as the key mediator of both functions and was accordingly replaced with Pro to demonstrate the consequences of the absence of a functional hinge on β-PGM structure and catalysis. Lastly, the model predicts that the paired cap domain residues His20 and Lys76 collaborate with Asp10 in the formation of a hydrogen bond network that stabilizes the liganded enzyme in the cap-closed conformation. The kinetic properties of site-directed mutants of His20 and Lys76 show that they too play a vital role in β-PGM catalysis.

MATERIALS AND METHODS

Enzymes and Reagents. α-D-[^{14}C-U]Glucose 1-phosphate [specific activity (SA) = 200 mCi/mmol] and D-[1-^{14}C]glucose 6-phosphate (SA = 49.3 mCi/mmol) were purchased from Perkin-Elmer Life Sciences to serve as standards in HPLC analysis. [^{14}C-U]Maltose (SA = 300 mCi/mmol) was purchased from American Radiolabeled Chemicals, Inc. Recombinant *Lactobacillus lactis* β-PGM was prepared according to the published procedure (*27*), and recombinant wild-type and mutant *Neisseria meningitidis* β-PGM was cloned, overexpressed, and purified in the same manner with a final yield of 20 mg/g of wet cell paste for wild-type and 20−30 mg/g for the mutants. Recombinant *L. lactis* maltose phosphorylase was prepared according to the published procedure (*28*). Fructose 6-phosphate kinase (EC 2.7.1.11) type VII from *Bacillus stearothermophilus*, pyruvate kinase (EC 2.7.1.40) type III from rabbit muscle, L-lactate dehydrogenase (EC 1.1.1.27) type XI from rabbit muscle, and glucose 6-phosphate dehydrogenase (EC 1.1.1.49) type IX from baker's yeast were purchased from Sigma-Aldrich. ATP, ADP, G6P, βG1P, PEP, NADP, and buffers were purchased from Sigma-Aldrich.

Synthesis of β-D-[^{14}C-U]Glucose 1-Phosphate. A 1.7 mL solution of 100 mM phosphate buffer (pH 7.2) containing 0.29 mM [^{14}C-U]maltose (SA = 300 mCi/mmol), 2 mM $MgCl_2$, and 4 μM maltose phosphorylase was incubated for 1 h at 25 °C. The reaction solution was passed through a 10 kDa filter to remove the enzyme and loaded onto a 1.5 cm × 25 cm Dowex-1 column. The column was eluted at 25 °C with 100 mL of deionized water to elute the maltose and glucose, followed by 130 mL of 0.6 M triethylammonium bicarbonate (pH 8) (flow rate of 200 mL/h). Column fractions (5 mL) were assayed for radioactivity using Ultima Gold liquid scintillation cocktail (Perkin-Elmer) with a Beckman LS 6500 multipurpose scintillation counter. The βG1P-containing fractions were combined and concentrated to 5 mL by rotary evaporation at 25 °C. The sample was twice diluted with 30 mL of deionized water and concentrated to remove triethylammonium bicarbonate. The resulting pellet was dissolved in 4 mL of deionized water to a final volume of 4.5 mL, to give a concentration of 92.6 μM (SA = 150 mCi/mmol) (yield of 84%). The sample was stored at −20 °C. The radiochemical purity of [^{14}C]βG1P was analyzed by HPLC using a Rainin Dynamax high-performance liquid chromatography system equipped with a CarboPac PA1 (Dionex) column (4 mm × 250 mm). The column was eluted at a flow rate of 1 mL/min with 2 mL of solvent A (54 mM NaOH and 100 mM sodium acetate), then with a linear gradient (15 mL) of solvent A to 53.7% solvent B (75 mM NaOH and 500 mM sodium acetate), and last with solvent B. Fractions (1 mL) were collected, and their radioactivity

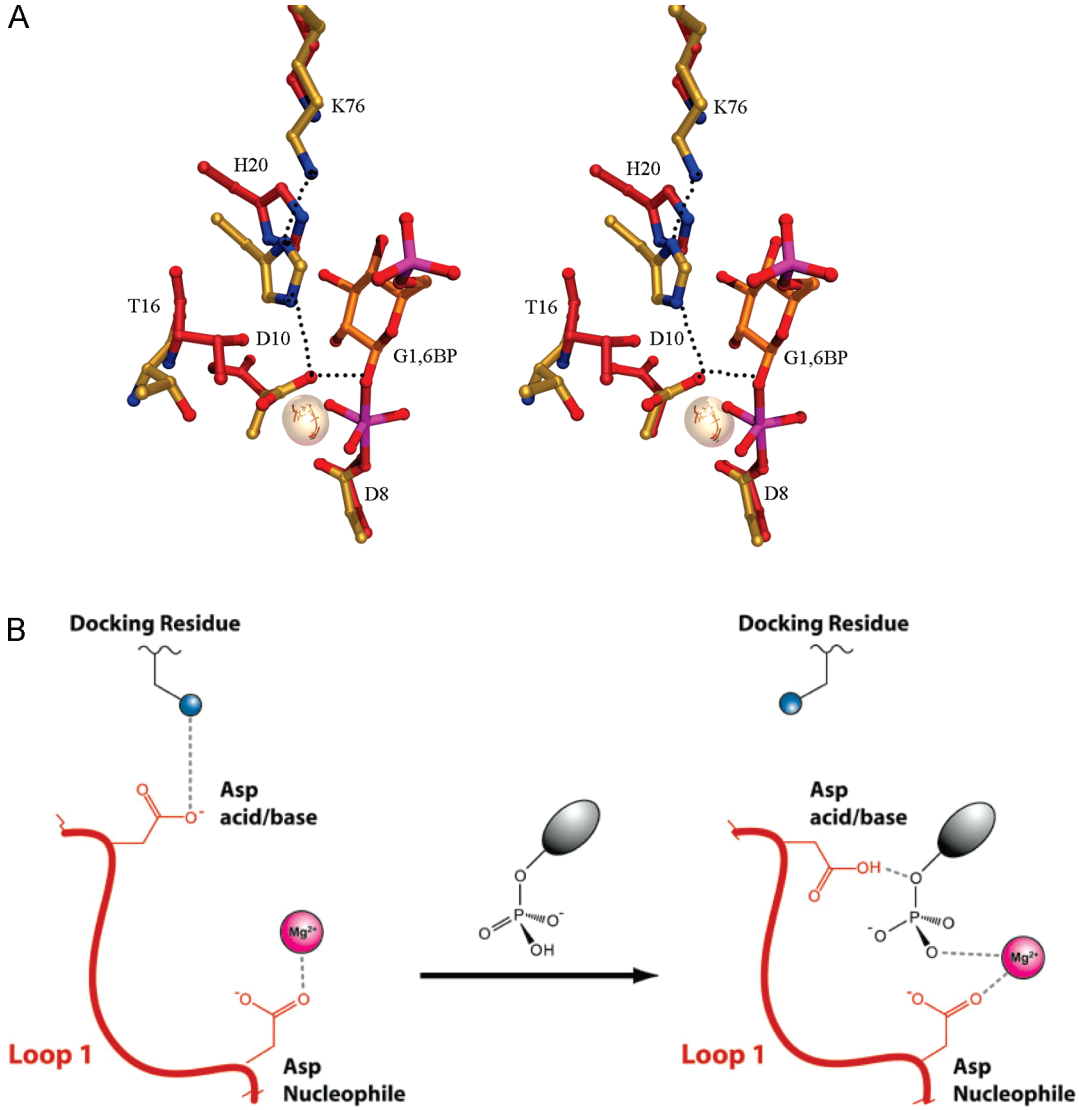

FIGURE 3: Changes in the active site between open and closed forms coordinated with ligand binding. (A) Stereoview of the overlay of the active sites of unliganded (red) and βG1,6bisP complex (gold) forms highlighting the hydrogen bond network (black dotted lines) among K76, H20, and D10 in the liganded form. βG1,6bisP is shown in ball-and-stick format and the Mg^{2+} cofactor as a silver sphere. (B) Schematic representation of the changes in orientation of D10 between the open (unliganded) and closed (liganded) forms.

content was determined by liquid scintillation counting. The retention time of the synthetic [^{14}C]-β-G1P was 9 min (radioactive purity of >95%). Desalting was accomplished by chromatography on a Sephadex G-10 column (1.2 cm × 120 cm) with deionized water as the eluent. The unlabeled βG1P was prepared by the same method, and the concentration of the final solution was determined spectrophotometrically using the β-PGM−glucose 6-phosphate dehydrogenase coupled reaction [1 mL of 50 mM K^+HEPES (pH 7.0) containing 2 mM $MgCl_2$, 0.4 mM NADP, 5 units of glucose 6-phosphate dehydrogenase, 10 nM β-PGM, and 5 μM βG1,6bisP, monitored at 340 nm and 25 °C; $\Delta\varepsilon = 6200$ M^{-1} cm^{-1}].

Synthesis of ^{14}C-Labeled and Unlabeled β-D-Glucose 1,6-Bisphosphate (βG1,6bisP). A 1.2 mL solution of 100 mM phosphate buffer (pH 7.2), 0.29 mM [^{14}C-U]maltose (SA = 300 mCi/mmol), 1 mM ATP, 2 mM $MgCl_2$, and 50 units/mL fructose 6-phosphate kinase (EC 2.7.1.11) type VII from *B. stearothermophilus* was incubated at 25 °C for 4 h and then passed through a 10 kDa filter to remove the enzyme. The filtrate was loaded onto a 1.5 cm × 25 cm Dowex-1 column, which was eluted at 25 °C using a 400 mL linear gradient of triethylammonium bicarbonate (from 0 to 0.8 M; pH 8.0) at a flow rate of 200 mL/h. Column fractions (5 mL) were assayed for radioactivity using Ultima Gold liquid scintillation cocktail (Perkin-Elmer) and a Beckman LS 6500 multipurpose scintillation counter. The βG1,6bisP-containing fractions (eluted at ~0.6−0.8 M triethylammonium bicarbonate) were combined and concentrated to 2 mL by rotary evaporation at 25 °C. The sample was diluted with 30 mL of deionized water and concentrated to a solid. This process was repeated several times to remove triethylammonium bicarbonate. The resulting white solid was dissolved in 3 mL of deionized water (51 μM [^{14}C-U]βG1,6bisP with a SA of 150 mCi/mmol; >95% radioactive purity; 51% yield) and stored at −20 °C. Complete desalting was accomplished by chromatography on a Sephadex G-10 column (1.2 cm × 120 cm) and with deionized water as the eluent. Unlabeled βG1,6bisP was prepared by the same method. The concentration of βG1,6bisP was determined spectrophotometrically using the β-PGM−glucose 6-phosphate dehydrogenase coupled reaction (vide infra).

Preparation of β-PGM Site-Directed Mutants. Mutant genes were prepared using a PCR-based strategy with the

pET3a-βPGM clone serving as a template and commercial oligonucleotides as primers. The PCR product was purified and following digestion with *Nde*I and *Bam*HI ligated to *Nde*I/*Bam*HI-linearized pET3a plasmid. Following confirmation of the mutant gene sequence by commercial DNA sequencing, the purified clone was used to transform competent *Escherichia coli* BL21(DE3) cells. The mutant proteins were purified to homogeneity (based on SDS−PAGE analysis) from cultured cells using the same method previously described for the preparation of wild-type β-PGM (*27*).

Steady-State Kinetic Constant Determination. All kinetic assays were conducted at 25 °C in 50 mM K^+HEPES (pH 7.0) containing 2 mM $MgCl_2$, unless stated otherwise. The formation of G6P was monitored by measuring the increase in absorbance at 340 nm ($\varepsilon = 6.2$ mM^{-1} cm^{-1}), resulting from the G6P dehydrogenase-catalyzed reduction of NADP. A specified volume of a β-PGM stock solution was added to a 1 mL solution containing βG1P, 50 mM K^+HEPES (pH 7.0), 2 mM $MgCl_2$, 5 μM βG1,6bisP, 0.2 mM NADP, and 2.5 units/mL G6P dehydrogenase. The kinetic data were analyzed using eq 1.

$$V_0 = V_m[S]/(K_m + [S]) \quad (1)$$

where [S] is the substrate concentration, V_0 is the initial velocity, V_m is the maximum velocity, and K_m is the Michaelis constant. The k_{cat} was calculated from the V_{max} and the enzyme subunit concentration determined by the Bradford method.

β-PGM-Catalyzed βG1,6bisP Hydrolysis. The steady-state kinetic constants of β-PGM-catalyzed βG1,6bisP hydrolysis were determined by measuring the initial velocity of product formation in reaction solutions initially containing wild-type or mutant β-PGM, 2 mM $MgCl_2$, and various concentrations of βG1,6bisP in 50 mM K^+HEPES (pH 7.0 and 25 °C). The formation of G6P was monitored using the G6P dehydrogenase−NADP coupled assay (vide supra), whereas the formation of orthophosphate was monitored using the PiBlue Phosphate Assay Kit (Invitrogen) according to the manufacturer's instructions.

Determination of Time Courses for Single-Turnover Reactions. Single-turnover experiments were performed at 25 °C using a rapid-quench instrument from KinTek Instruments equipped with a thermostatically controlled circulator. A typical experiment was carried out by mixing 13 μL of buffer A [50 mM K^+HEPES (pH 7.0) and 2 mM $MgCl_2$] containing β-PGM and 14 μL of buffer A containing [^{14}C-U]βG1,6bisP or [^{14}C-U]βG1P and βG1,6bisP. The reaction was quenched after a specified period of time with 193 μL of 1 M NaOH. The quenched reaction mixture was passed through a 5 kDa filter to remove the enzyme and loaded onto a Rainin Dynamax high-performance liquid chromatography (HPLC) system equipped with a CarboPac PA1 (Dionex) column (4 mm × 250 mm). The column was eluted at 1 mL/min with 2 mL of solvent A (54 mM NaOH and 100 mM sodium acetate), then with a linear gradient (15 mL) of solvent A to 53.7% solvent B (75 mM NaOH and 500 mM sodium acetate), and last with solvent B. Fractions (1 mL) were collected, and their radioactivity was determined by liquid scintillation counting. The retention times of βG1P, G6P, and βG1,6bisP are 8, 15, and 21 min, respectively. The radioactivity associated with the respective [^{14}C]βG1P, [^{14}C]G6P, and [^{14}C]βG1,6bisP fractions was used to calculate the mole fraction of each species present in the reaction mixture at termination. The observed rate constants for the single-turnover reactions were obtained by fitting the time course data to first-order eqs 2 and 3 using KaleidaGraph.

$$[P]_t = [P]_{max}(1 - e^{kt}) \quad (2)$$

$$[S]_t = [S]_{max} - [[P]_{max}(1 - e^{-kt})] \quad (3)$$

where $[P]_t$ and $[S]_t$ are the product and substrate concentrations at time t, respectively, $[P]_{max}$ is the product concentration at equilibrium, $[S]_{max}$ is the initial concentration of substrate, and k is the first-order rate constant.

X-ray Crystallographic Determination of the β-PGM T16P Structure. Crystallization conditions for the β-PGM T16P mutant were identified in hanging-drop, vapor-diffusion experiments using the Index Screen (Hampton Research). Although 5 mM β-glucose 1-phosphate and 5 mM β-glucose 1,6-bisphosphate were included in the crystallization buffer to allow formation of a Michaelis complex, extensive screening did not yield a liganded complex or crystals of protein in the cap-closed form. Initial screening hits were refined to yield final crystallization conditions using equal parts (1 μL each) of T16P β-PGM (15 mg/mL) in 50 mM HEPES (pH 7.5), 10 mM $MgCl_2$, and 1 mM DTT and well solution containing 25% PEG, 0.2 M NaCl, and 100 mM BisTris (pH 6.0). Small crystals grew in 7 days to final dimensions of 0.3 mm × 0.1 mm × 0.05 mm. X-ray diffraction data were collected on beamline X12C (Brookhaven National Laboratory, Upton, NY). The crystals were protected for cryo-crystallography with Paratone N before being flash-cooled to 100 K in a gaseous N_2 stream. Data were collected to 2.7 Å resolution and processed using DENZO and SCALEPACK (*29*). Data collection statistics are reported in Table 1.

The structure of T16P β-PGM was determined by molecular replacement. Initial trials used the structures of wild-

Table 1: Crystallographic Data Collection and Refinement Statistics

Data Collection Statistics	
resolution (last shell) (Å)	50.00−2.70 (2.80−2.70)
X-ray source	NSLS X12C
wavelength (Å)	1.000
space group	$P2_12_12_1$
unit cell dimensions (Å)	$a = 54.478$, $b = 57.656$, $c = 77.899$
no. of reflections observed (unique)	39160 (7122)
completeness (%)	99.3
R_{merge}[a] (%)	15.1 (54.7)
$I/\sigma(I)$	14.7 (3.3)
redundancy	5.5 (5.4)
Refinement Statistics	
no. of protein/water atoms per asu	1706/62
no. of Mg ions per asu	1
no. of reflections (work/free)	6778/678
R_{work}/R_{free} (%)	20.1/28.0
resolution (Å)	39.6−2.70
average B factor (Å^2)	32.6
protein	32.5
Mg^{2+}	40.2
water	35.3
Wilson B factor	56.8
root-mean-square deviation	
bond lengths (Å)	0.008
bond angles (deg)	1.030

[a] $R_{merge} = \sum_{hkl}\sum_i|I_{hkl,i} - \langle I_{hkl}\rangle|/\sum_{hkl}\sum_i|I_{hkl,i}|$, where $\langle I_{hkl}\rangle$ is the mean intensity of the multiple $I_{hkl,i}$ observations for symmetry-related reflections.

Table 2: Steady-State Kinetic Constants for Wild-Type and Mutant β-PGM Measured Using Assay Solutions Containing Varying Concentrations of βG1P, 5 μM βG1,6bisP, 2 mM $MgCl_2$, 0.2 mM NADP, and 2.5 Units/mL Glucose 6-Phosphate Dehydrogenase in 50 mM K^+HEPES (pH 7.0 and 25 °C)

β-PGM	K_m (μM)	k_{cat} (s^{-1})	k_{cat}/K_m (M^{-1} s^{-1})
N. meningitidis WT[a]	2.6 ± 0.3	20 ± 2	8×10^6
N. meningitidis D10A[a]	ND[b]	<0.001	ND[b]
N. meningitidis D10E[a]	ND[b]	<0.001	ND[b]
L. lactis WT	31 ± 2	175 ± 5	6×10^6
L. lactis D10N	ND[b]	<0.001	ND[b]
L. lactis D10S	ND[b]	<0.001	ND[b]
L. lactis D10C	ND[b]	<0.001	ND[b]
L. lactis T16P	4.8 ± 0.3	0.026 ± 0.001	5×10^3
L. lactis H20Q	45 ± 1	21.9 ± 0.1	5×10^5
L. lactis H20N	170 ± 10	0.62 ± 0.02	4×10^3
L. lactis H20A	41 ± 3	0.026 ± 0.004	6×10^2
L. lactis K76A	66 ± 1	1.56 ± 0.01	2×10^4

[a] Measured using 50 μM αG1,6bisP in place of 5 μM βG1,6bisP. [b] Not determined.

type β-PGM in the cap-open (PDB entry 1LVH) or cap-closed (PDB entry 1O08) conformations as search models with PHASER (*30*). Only the cap-open form yielded a correct solution, which was confirmed by subsequent refinement using PHENIX (*31*). The refinement protocol consisted of one round of rigid body refinement, followed by individual atomic coordinate and isotropic temperature factor refinement, alternating with cycles of model building in COOT (*32*). Water molecules visible as spherical peaks in $|F_o| - |F_c|$ electron density maps contoured at 3.0σ were added to the model. The quality of the model was assessed by geometry analysis with MOLPROBITY (*33*). Final refinement and model quality statistics are given in Table 1.

The D10N mutant was crystallized from 0.1 M Tris-HCl (pH 8.5) and 2 M ammonium sulfate. Plate-shaped crystals (0.8 mm × 0.2 mm × 0.1 mm) grew in 10−14 days. The cryoprotectant consisted of mother liquor supplemented with 20% glycerol. The crystals diffracted to 2.1 Å resolution. Although molecular replacement using PHASER gave a successful solution ($R_{factor} < 40$), the data were incomplete due to crystal decay. Attempts to refine the data set were unsuccessful.

RESULTS AND DISCUSSION

Evaluation of the Contribution of Asp10 to β-PGM Catalysis. To determine the extent to which Asp10 contributes to catalytic efficiency, Ala10, Ser10, Cys10, Asn10, and Glu10 β-PGM mutants (prepared from either the *N. meningitidis* β-PGM or *L. lactis* β-PGM as dictated by successful gene expression) were evaluated as catalysts of the mutase reaction depicted in Figure 2B. Reaction solutions, initially containing 5 μM βG1,6bisP, 100 μM βG1P, 2 mM $MgCl_2$, 50 mM K^+HEPES (pH 7.0, 25 °C), and 5 μM β-PGM mutant, were monitored for G6P formation over a 30 min period using the spectrophotometric assay described in Materials and Methods. G6P formation was not observed in any of the reactions, indicating a maximum turnover rate that is catalytically insignificant (i.e., $< 1 \times 10^{-3}$ s^{-1}) (Table 2).

The ability of the β-PGM mutant to catalyze Asp8 phosphorylation with βG1,6bisP was tested by measuring the time course for a single-turnover reaction (Scheme 1). Accordingly, 40 (or 5) μM [^{14}C]βG1,6bisP was reacted with

Scheme 1

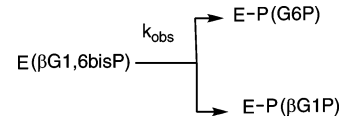

40 μM *L. lactis* D10N β-PGM in 2 mM $MgCl_2$ and 50 mM K^+HEPES (pH 7.0, 25 °C). Following a 90 min incubation period, the quenched reaction mixture was analyzed by HPLC to reveal only unconsumed reactant and no [^{14}C]G6P or [^{14}C]βG1P. Similarly, *L. lactis* D10S β-PGM (170 μM) and D10C β-PGM (300 μM) failed to catalyze a single-turnover reaction with βG1,6bisP (50 μM). In contrast, the time course for the reaction of 40 μM wild-type *L. lactis* β-PGM with 5 μM [^{14}C]βG1,6bisP (measured by rapid quench) shows that the reaction is complete within 3 ms (the mixing time of the instrument) (Figure 4A). This defines a minimum turnover rate of 400 s^{-1} (Table 2). The lack of observable activity of the Asp10 mutants indicates that Asp10 is required for catalysis, assuming that binding is similar to that observed in the wild-type enzyme.[2]

The X-ray structure determination of D10N β-PGM was undertaken in hopes of obtaining a snapshot of the liganded mutant enzyme. The crystals that were grown diffracted to 2.1 Å resolution, and an initial molecular replacement solution was achieved. However, the crystal decay that had occurred during data collection resulted in a data set that did not lend itself to satisfactory refinement. Although the success of crystallization and phasing via molecular replacement supports the conservation of the native fold in the mutant, the refinement statistics are not sufficient for publication of the structure.

The Hinge Residue Thr16 Plays a Critical Role in L. lactis β-PGM Mutase Catalysis. The switch from the cap-open to cap-closed conformers is accompanied by a rotation of the φ and ψ dihedrals of −9.0 and 26.5°, −95.1 and 41.6°, and 14.9 and −12.1°, respectively, for the bonds between linker residues Thr14 and Asp15, Asp15 and Thr16, and Thr16 and Ala17, respectively (see Figures 1B and 3A). Dyndom (*35*) was used to identify Asp15 and Thr16 as the residues that undergo the greatest change in dihedral angle. This finding, combined with the observation that in the cap-open conformer, the Asp10 side chain carboxylate group binds to the Thr16 backbone amide NH group via a hydrogen bond, prompted the selection of Thr16 for replacement with Pro. Notably the φ and ψ angles at Thr16 are in the same portion of Ramachandran space for both cap-open and cap-closed conformers of the enzyme. Thus, it is expected that the replacement with Pro will limit the dynamic motion by constraint of the φ angle at the mutation site to −60° and thus restrict interconversion between the cap-open conformer and the catalytically active cap-closed conformer. In addition, it is expected that the removal of the hydrogen bond between

[2] A reviewer pointed out that because the Asp10 side chain engages in a hydrogen bond with the C(1)O group of βG1,6bisP [and presumably with the C(6)OH group of βG1P] the Asp 10 mutants might not be able to bind the substrate. We consider this unlikely, because this hydrogen bond is one among numerous substrate binding interactions. Moreover, it is likely that the hydrogen bond is preserved in the D10N mutant. The role that the Asn10 residue cannot fill is that of a general acid/base catalyst. Notably, our conclusions rest on the assumption that β-glucose 1,6-bisphosphate binds to the D10N variant.

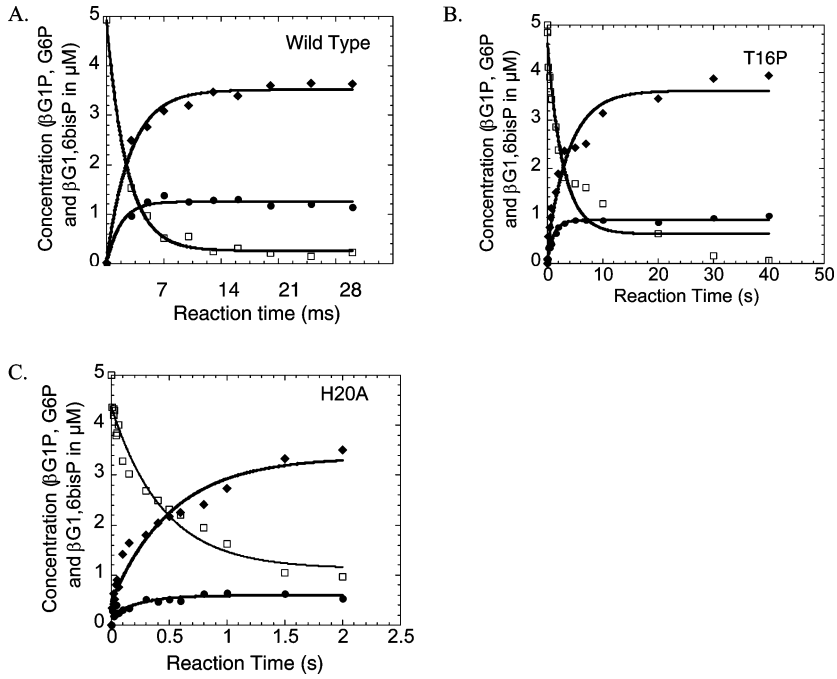

FIGURE 4: Time course for the single-turnover reaction of 40 μM wild-type *L. lactis* β-PGM (A), 20 μM T16P β-PGM (B), and 40 μM H20A β-PGM (C) with 5 μM [^{14}C]βG1,6bisP in 50 mM K^+HEPES containing 2 mM $MgCl_2$: [^{14}C]βG1,6bisP (□), [^{14}C]βG6P (◆), and [^{14}C]βG1P (●).

Table 3: Apparent Rate Constants of Wild-Type and Mutant *L. lactis* β-PGM (20−40 μM)-Catalyzed Single-Turnover Reactions of 5 μM [^{14}C]βG1,6bisP[a]

β-PGM (μM)	k_{obs}(βG1P) (s^{-1})	k_{obs}(G6P) (s^{-1})	k_{obs}(βG1,6bisP) (s^{-1})
wild-type (40)	>400	>400	>400
T16P (20)	0.9 ± 0.2	0.8 ± 0.1	0.8 ± 0.1
H20A (40)	4 ± 1	1.9 ± 0.4	2.2 ± 0.4

[a] The k_{obs} values for the formation of [^{14}C]βG6P or [^{14}C]βG1P and the consumption of [^{14}C]βG1,6bisP were obtained by fitting the individual sets of time course data to first-order rate equations.

Thr16 and Asp10 would impair the enzyme's ability to pin the Asp10 to the linker and hence, outside the active site, in the cap-open conformer. Thus, via examination of the structure and the catalytic properties of the T16P mutant, the importance of a functional hinge in β-PGM catalysis was probed.

The catalytic properties of *L. lactis* T16P β-PGM were evaluated using steady-state and transient-state kinetic methods. First, the time course for the single-turnover reaction of [^{14}C]βG1,6bisP was measured by rapid quench to define a k_{obs} of 0.8 s^{-1} (Figure 4B and Table 3). Comparison to a k_{obs} of >400 s^{-1} for wild-type *L. lactis* β-PGM shows that the mutation causes a significant reduction in the efficiency of the autophosphorylation step. This indicates that the altered hinge region may disfavor formation of the cap-closed conformer and/or that the alignment of the surfaces at the domain−domain interface of the cap-closed conformer might be affected.

Second, we used steady-state techniques to measure the k_{cat} values for wild-type and T16P *L. lactis* β-PGM-catalyzed hydrolysis of βG1,6bisP to approximate the rate of hydrolysis of the phospho-Asp8 that occurs in the absence of βG1P. Our working assumption is that β-PGM-catalyzed hydrolysis of βG1,6bisP occurs via the phosphorylation of Asp8

Scheme 2

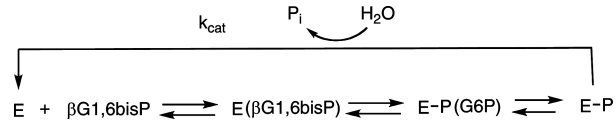

Table 4: Steady-State Kinetic Constants of *L. lactis* β-PGM-Catalyzed βG1,6bisP Hydrolysis in 50 mM K^+HEPES (pH 7.0, 25 °C) Containing 2 mM $MgCl_2$ and βG1,6bisP at Various Concentrations

β-PGM	K_m (μM)	k_{cat} (s^{-1})
wild-type	0.63 ± 0.07	0.0298 ± 0.008
H20N	1.49 ± 0.09	0.0303 ± 0.0005
H20A	2.6 ± 0.1	0.0197 ± 0.003
T16P	10 ± 1	0.38 ± 0.01

followed by hydrolysis of the phospho-Asp8 to form orthophosphate (P_i) and G6P and regenerate the Asp8 (Scheme 2).[3]

For the wild-type β-PGM, the phosphorylation step occurs with a k_{obs} of >400 s^{-1} (Table 3), whereas the k_{cat} value measured for the βG1,6bisP hydrolysis reaction is 0.03 s^{-1} (Table 4). Therefore, we conclude that phospho-Asp8 hydrolysis is the rate-limiting step, and that the k_{cat} of 0.03 s^{-1} approximates the rate constant governing this step. The k_{obs} of 0.8 s^{-1} measured for T16P β-PGM-catalyzed Asp8 phosphorylation with βG1,6bisP is only 2-fold greater than the k_{cat} of 0.38 s^{-1} measured for T16P β-PGM-catalyzed hydrolysis of βG1,6bisP (Table 4). Thus, mutation of the hinge reduces the rate constant governing phosphoryl transfer from βG1,6bisP to Asp8 yet increases the rate constant governing the phosphoryl transfer from phospho-Asp8 to solvent.

[3] An alternative mechanism for hydrolysis of the βG1,6bisP cannot, in the absence of experimental proof, be ruled out. However, such a reaction pathway would require an active site-bound water molecule to compete with the Asp8 for in-line displacement of G6P from bound βG1,6bisP, which we find to be unlikely given the structure and function of the active site catalytic scaffold.

Scheme 3

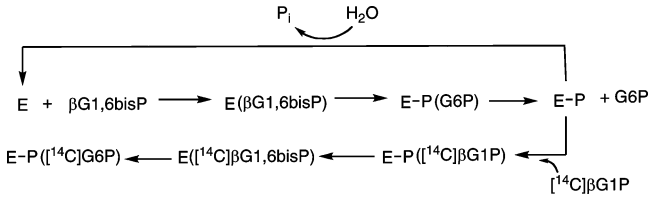

How then does the rate constant for phospho-Asp8 hydrolysis compare with the rate constant defining phosphoryl transfer from phospho-Asp8 to βG1P? The steady-state k_{cat} of 175 s^{-1} (Table 2) measured for the multistep conversion of βG1P to G6P (Figure 2B) sets the minimum value for this rate constant, and therefore, the βG1P versus water solvent discrimination factor observed for phosphorylated wild-type β-PGM is greater than or equal to 175 s^{-1}/0.03 s^{-1} = 5800. Clearly, in the presence of βG1P, wild-type β-PGM does not lose the phosphoryl group from phospho-Asp8 to solvent.

The k_{cat} of 0.026 s^{-1} measured for the multistep conversion of βG1P to G6P catalyzed by T16P β-PGM defines the minimum value for the rate constant for the transfer of phospho-Asp8 to βG1P. The ratio of the k_{cat} of 0.026 s^{-1} for the full catalytic cycle to the k_{cat} of 0.38 s^{-1} for βG1,6bisP hydrolysis catalyzed by T16P suggests that transfer of the phospho-Asp8 to water might effectively compete with the transfer to the substrate βG1P. To test this possibility, additional kinetic experiments were carried out. First, continual monitoring of a reaction solution initially containing 5 μM T16P, 100 μM βG1P, and 5 μM βG1,6bisP revealed that only 14 μM G6P was formed. Given that G6P formation is thermodynamically favored, this result suggested that the mutant enzyme is not able to convert all of the βG1P. Such would be the case if water competes with the βG1P for the phosphorylated enzyme. By carrying out the reaction with [^{14}C]βG1P, we were able to monitor its conversion to [^{14}C]G6P as a function of added unlabeled βG1,6bisP. The reaction steps are illustrated in Scheme 3 to show that if a molecule of phosphorylated enzyme loses the phosphoryl group to solvent it must be replaced by consuming an additional molecule of βG1,6bisP. If there is no surplus βG1,6bisP, catalysis will terminate. This is clearly evident in the time course measured for the reaction of 20 μM T16P β-PGM with 5 μM [^{14}C]βG1P and 5 μM βG1,6bisP (Figure 5B). Whereas the analogous reaction carried out with wild-type β-PGM proceeds to 100% completion (Figure 5A), the T16P β-PGM-catalyzed reaction proceeds to only 10% completion. By carrying out the T16P β-PGM-catalyzed reaction in the presence of excess βG1,6bisP (50 μM), we show that the reaction proceeds further toward completion [40% (Figure 5C)]. Overall, these results show that water is able to effectively compete with the substrate for phospho-Asp8 in the case of the T16P β-PGM mutant but not in the case of the wild-type enzyme.

X-ray Structure Determination of T16P β-PGM. The replacement of hinge residue Thr16 with Pro results in a 500-fold reduction in the rate constant for Asp8 phosphorylation by βG1,6bisP, a 6700-fold reduction in the "apparent" rate constant for cycling of the phosphorylated enzyme to convert βG1P to G6P, and a 13-fold increase in the estimated rate constant for phosphoryl transfer from the phospho-Asp8 to water. The corresponding structural consequences of the mutation were evaluated by X-ray crystallography.

Exhaustive crystallization screening identified two distinct crystal forms, both of which were consistent with an open conformation of the core and cap domains (based on the initial model obtained via molecular replacement). The form that diffracted to higher resolution (2.7 Å) was used for structure determination. The resulting model was refined to completion to yield the T16P β-PGM(Mg^{2+}) structure presented here. The structure shows good electron density overall, and that observed at the site of mutation is shown in Figure 6. Comparison of the T16P β-PGM(Mg^{2+}) structure with that of the wild-type cap-open conformer observed for the phosphorylated β-PGM(Mg^{2+}) complex reveals that the T16P β-PGM mutant is slightly more "open", with a 6.5° angle of rotation between the cap and the core domains. The positions of the catalytic residues are conserved in the two cap-open structures with the exception of the Asp10 general acid/base (Figure 7A), which moves from a position where it forms a hydrogen bond to hinge residues in the wild-type β-PGM to inside the active site in the mutant enzyme. Least-squares fitting of the mutant structure with that of the liganded cap-closed conformer of the wild-type enzyme [viz. β-PGM(Mg^{2+})(βG1,6bisP)] (Figure 7B) shows that the respective Asp10 carboxylate groups are in the proximity of one another (Figure 7C).

Together, these findings suggest that the removal of the potential for hydrogen bond interaction between the Asp10 carboxylate and the backbone amide NH group at position 16 destabilizes the binding interaction of Asp10 with the hinge and that this in turn results in the Asp10 carboxylate group occupying a position in the active site where it can potentially function to activate a water molecule for attack at the phospho-Asp8. This is consistent with the findings of the kinetic analysis, which showed that the rate constant for phosphoryl transfer from the phospho-Asp8 to water is 13-fold larger for the T16P mutant than for wild-type β-PGM.

Kinetic analysis also shows that replacement of Thr16 with Pro impairs Asp8 phosphorylation by βG1,6bisP and phosphoryl transfer from the phospho-Asp8 to the substrate βG1P. Both reaction steps proceed from the cap-closed conformer. We speculate that the restriction imposed on the ϕ angle at the mutation site might disfavor formation of the cap-closed conformer and/or perturb the alignment of the domain interface. Unfortunately, we did not succeed in generating crystals of the liganded mutant for structure determination of the cap-closed conformer to confirm this hypothesis.

Cap Domain Residues His20 and Lys76 Play a Critical Role in β-PGM Mutase Activity. The hydrogen bond network observed in the crystal structure of the cap-closed conformer of the β-PGM(Mg^{2+})(βG1,6bisP) complex (Figure 3) suggests a cooperative interaction among the reactant C(1)O group, the Asp10 general acid/base, and cap-domain residues His20 and Lys76. This network ensures the proper position of Asp10 in the context of the substrate-mediated closure of the cap domain over the core domain. To test the contributions made by hydrogen bond partners His20 and Lys76 to β-PGM catalysis, the kinetic properties of site-directed mutants were evaluated.

Replacement of the His20 side chain with Ala eliminates the potential for formation of this hydrogen bond network. This is expected to impair Asp8 phosphorylation by βG1,6bisP

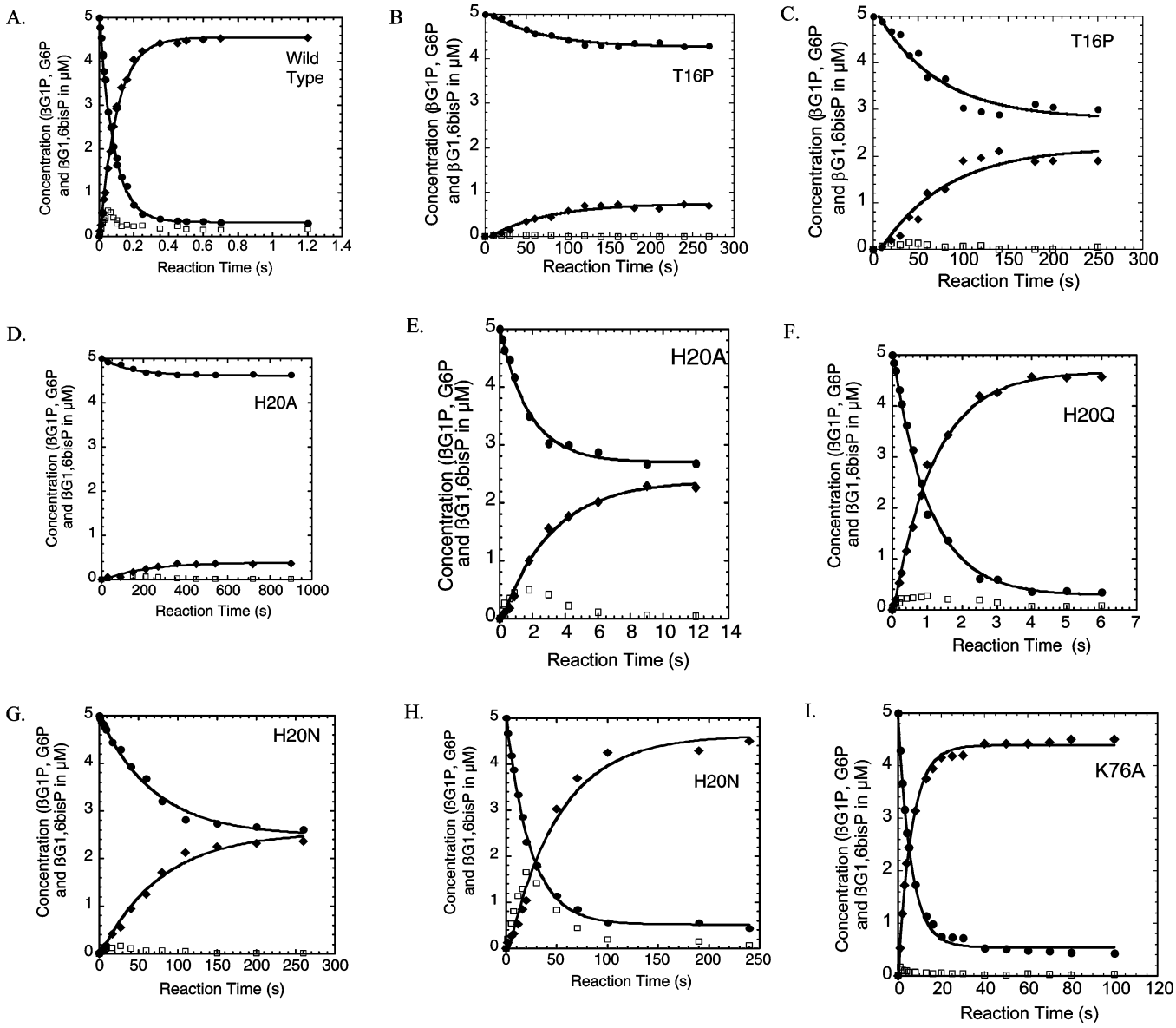

FIGURE 5: Time course for a single-turnover reaction of 5 μM [^{14}C]βG1P in 50 mM K$^+$HEPES buffer containing 2 mM $MgCl_2$ and (A) 40 μM wild-type β-PGM and 5 μM βG1,6bisP, (B) 20 μM T16P β-PGM and 5 μM βG1,6bisP, (C) 20 μM T16P β-PGM and 50 μM βG1,6bisP, (D) 40 μM H20A β-PGM and 5 μM βG1,6bisP, (E) 40 μM H20A β-PGM and 50 μM βG1,6bisP, (F) 40 μM H20Q β-PGM and 5 μM βG1,6bisP, (G) 40 μM H20N β-PGM and 5 μM βG1,6bisP, (H) 40 μM H20N β-PGM and 50 μM βG1,6bisP, and (I) 40 μM K76A β-PGM and 5 μM βG1,6bisP: [^{14}C]βG1,6bisP (□), [^{14}C]βG6P (◆), and [^{14}C]βG1P (●).

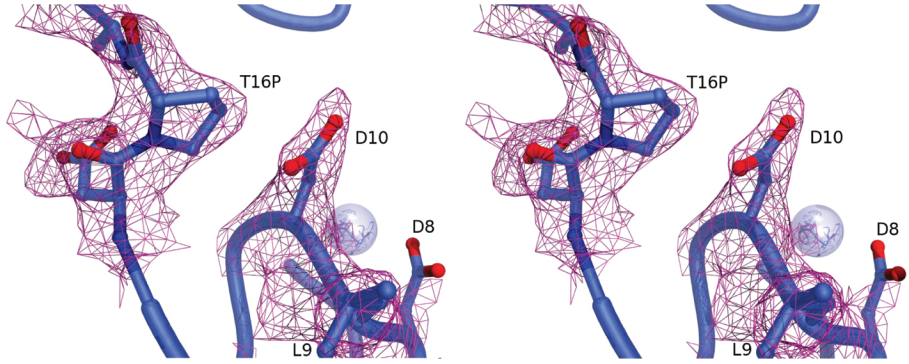

FIGURE 6: Structure of T16P β-PGM. (A) Stereoview of the active site of T16P β-PGM with composite-omit electron density map ($2F_o - F_c$ contoured at 1σ) shown as magenta cages at the site of mutation and at the general acid/base residue Asp10. The Mg^{2+} cofactor is shown as a silver sphere.

and phosphoryl transfer from the phospho-Asp8 to the substrate βG1P. The single-turnover rate constant, "k_{obs}", measured for H20A β-PGM-catalyzed phosphorylation of the Asp8 with [^{14}C]βG1,6bisP is 2 s^{-1} (Figure 4C and Table 3). The >200-fold reduction in the rate constant for the Asp8 phosphorylation step is no doubt coupled with a comparable

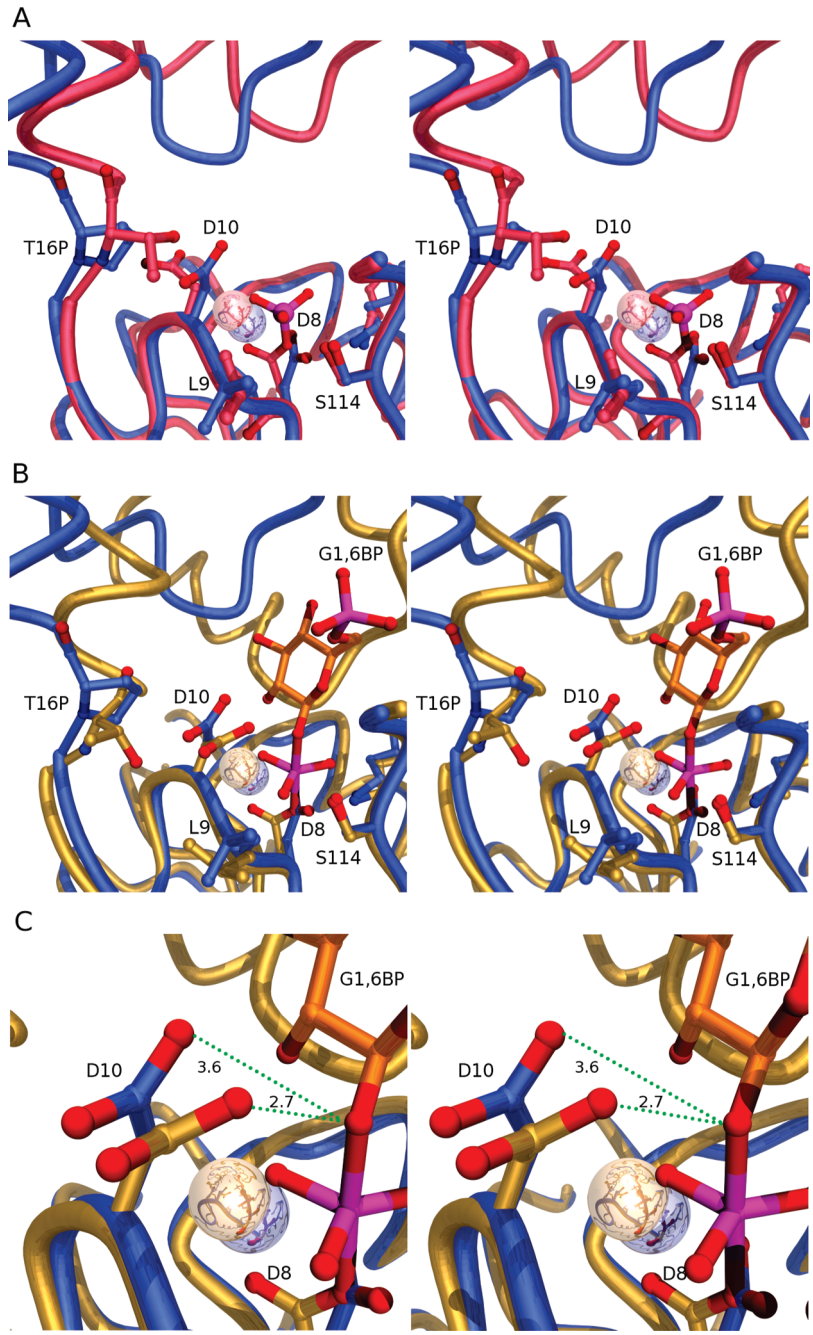

FIGURE 7: Structural comparison of T16P β-PGM (blue) with unliganded (open, red) and liganded wild-type β-PGM structures (closed, gold) shows that the overall structure of T16P β-PGM (blue) is in the open form. Examination of the active site overlay with the open form (A) and the closed form (B and close-up in C) demonstrates that the general acid/base Asp10 is positioned as it is in the wild-type closed form.

reduction in the rate constant governing the phosphoryl transfer from the phospho-Asp8 to βG1P. Indeed, the steady-state k_{cat} of 0.026 s^{-1} measured for the catalyzed conversion of βG1P to G6P in the presence of βG1,6bisP is reduced ~7000-fold in the H20A mutant (Table 2).

The consequence of the reduction in the efficiency of phosphoryl transfer from the mutant phospho-Asp8 was revealed by the time courses measured for the reaction of 40 μM H20A β-PGM with 5 μM [^{14}C]βG1P and 5 or 50 μM βG1,6bisP (Figure 5D,E). These time courses show that the reaction proceeds to only 10 or 50% completion, respectively, which demonstrates that water is successfully competing for the phospho-Asp8. The k_{cat} of 0.02 s^{-1} for H20A β-PGM-catalyzed hydrolysis of βG1,6bisP, which we assume estimates the rate constant for the transfer of the phosphoryl group from the phospho-Asp8 to water, is comparable to the steady-state k_{cat} of 0.026 s^{-1} measured for the catalyzed conversion of βG1P to G6P (Table 4).

The imidazole ring of the H20 residue provides two hydrogen bond donors and/or acceptors: one for the Asp10 side chain and the other for the Lys76 side chain. To explore the impact of substituting His20 with residues that might form one but not both hydrogen bonds, we examined the kinetic properties of the H20Q and H20N β-PGM mutants. *In silico* modeling using the X-ray structure of the β-PGM(Mg^{2+})(βG1,6bisP) complex indicated that the Gln side chain can potentially form a hydrogen bond with the Asp10 side chain and that the Asn side chain can potentially

Table 5: Apparent Rate Constants of the Wild-Type and Mutant *L. lactis* β-PGM (40 or 20 μM)-Catalyzed Single-Turnover Reactions of [^{14}C]βG1P (5 μM) in the Presence of βG1,6bisP (5 or 50 μM)[a]

β-PGM	[βG1,6bisP] (μM)	k_{obs}(βG1P) (s^{-1})	k_{obs}(βG6P) (s^{-1})	G6P/βG1P
wild-type	5	12.2 ± 0.3	9.3 ± 0.4	10
T16P[b]	50	0.014 ± 0.002	0.014 ± 0.002	0.6
H20Q	5	0.96 ± 0.04	0.78 ± 0.04	10
H20N	50	0.042 ± 0.002	0.018 ± 0.002	10
H20A	50	0.0055 ± 0.0004	0.0029 ± 0.003	1
K76A	5	0.164 ± 0.006	0.157 ± 0.004	10

[a] The k_{obs} values for [^{14}C]G6P or [^{14}C] βG1,6bisP formation and [^{14}C]βG1P consumption were obtained by fitting the individual sets of time course data to first-order rate eq 2 or 3. [b] The enzyme concentration was 20 μM.

form a hydrogen bond with the Lys76 side chain (but not with that of Asp10). The steady-state kinetic analysis of *L. lactis* H20Q and H20N β-PGM-catalyzed conversion of βG1P to G6P in the presence of βG1,6bisP revealed 8- and 300-fold diminutions in k_{cat}, respectively (Table 2). The H20Q β-PGM (Figure 5F) is significantly more effective in distinguishing βG1P as the phosphate acceptor than is H20N β-PGM (Figure 5G,H), which in turn is more effective than H20A β-PGM (Figure 5D,E). The rate constant governing the phosphoryl transfer to water is essentially unchanged in the H20N mutant (the H20Q mutant was not tested) (Table 4).

Lastly, we examined the contribution of the conserved cap domain residue Lys76, which positions His20 via a hydrogen bond and contributes to the hydrogen bond network. Steady-state kinetic measurements of the conversion of βG1P to G6P in the presence of βG1,6bisP showed that the k_{cat} for the *L. lactis* K76A mutant is reduced 100-fold from that of the wild-type β-PGM (Table 2). Nevertheless, the time course for the single-turnover reaction of [^{14}C]βG1P (5 μM) and βG1,6bisP (5 μM) catalyzed by K76A β-PGM (40 μM) shows complete conversion of the substrate (Figure 5I and Table 5). These results show that Lys76 contributes significantly to β-PGM catalysis, but to a lesser extent than His20 does.

CONCLUSION

β-PGM evolved within an enzyme family that is dominated by phosphatases. It shares with these phosphatases a catalytic mechanism that is built on the use of an Asp to function in nucleophilic catalysis and an Asp to function in general acid/base catalysis. Whereas the Asp10 general acid/base of β-PGM moves into the active site when the cap and core domains associate and then moves out of the active site when they dissociate, the Asp general acid/base of the phosphatase remains in the core domain active site where it is held in place by a nearby electropositive residue (*34*). Thus, whereas β-PGM relies on substrate-induced cap domain closure to position the Asp, the phosphatase does not and is therefore able to constitutively activate a water molecule derived from solvent for reaction.

Asp10 was shown to be essential for β-PGM-catalyzed phosphorylation of the Asp8 nucleophile, and although it is not demonstrated, it is reasonable to assume that it also plays an important role in the ensuing phosphoryl transfer step. By mutating the hinge, we were also able to show that Asp10 will enter the core domain active site in the cap-open conformer. The observed increase in the rate of phospho-Asp8 hydrolysis in the linker mutant is consistent with the greater availability of the Asp10 to bind and activate a water molecule in the cap-open conformer. The mutation of the hinge significantly reduces the efficiency of Asp8 phosphorylation by βG1,6bisP and the efficiency of βG1P phosphorylation by the phospho-Asp8. We were unable to determine the structure of the hinge mutant in the cap-closed conformer, and therefore, we can only speculate that productive domain−domain association is impaired by the mutation.

The relationship between domain−domain association and catalytic efficiency was further explored by mutating the paired cap domain residues His20 and Lys76 to disrupt the hydrogen bond network that includes the βG1,6bisP C(1)O group and the Asp10 side chain. The cap domain mutants displayed significantly reduced efficiency in catalysis of Asp8 phosphorylation by βG1,6bisP and of βG1P phosphorylation by the phospho-Asp8 but no change in efficiency of catalyzed phospho-Asp8 hydrolysis. The hydrogen bond network and the other hydrogen bond interactions that occur between the G6P moiety and the cap domain are suggested to stabilize the cap-closed conformer and thus form the basis for the substrate-induced cap domain closure.

Taken together, these results present a picture that is consistent with the proposal that β-PGM is a very efficient mutase and very inefficient phosphatase because catalysis must occur from the cap-closed conformation, and only βG1P (not solvent water) can stabilize the phosphorylated enzyme in the cap-closed conformation.

ACKNOWLEDGMENT

We thank Dr. Nicholas Silvaggi and Dr. Zhibing Lu for assistance with figure preparation and Kelly Daughtry for assistance with data collection. Data for this study were measured at Beamline X12C of the National Synchrotron Light Source, Brookhaven National Laboratory.

REFERENCES

1. Dai., J. B., Liu, Y., Ray, W. J., Jr., and Konno, M. (1992) The crystal structure of muscle phosphoglucomutase refined at 2.7-angstrom resolution. *J. Biol. Chem. 267*, 6322–6337.
2. Wang, Y., Wei, Z., Liu, L., Cheng, Z., Lin, Y., Ji, F., and Gong, W. (2005) Crystal structure of human B-type phosphoglycerate mutase bound with citrate. *Biochem. Biophys. Res. Commun. 331*, 1207–1215.
3. Lahiri, S. D., Zhang, G., Dunaway-Mariano, D., and Allen, K. N. (2002) Caught in the act: The structure of phosphorylated β-phosphoglucomutase from *Lactococcus lactis*. *Biochemistry 41*, 8351–8359.
4. Silvaggi, N. R., Zhang, C., Lu, Z., Dai, J., Dunaway-Mariano, D., and Allen, K. N. (2006) The X-ray crystal structures of human α-phosphomannomutase 1 reveal the structural basis of congenital disorder of glycosylation type 1a. *J. Biol. Chem. 281*, 14918–14926.
5. Jolly, L., Ferrari, P., Blanot, D., Van Heijenoort, J., Fassy, F., and Mengin-Lecreulx, D. (1999) Reaction mechanism of phosphoglucosamine mutase from *Escherichia coli*. *Eur. J. Biochem. 262*, 202–210.
6. Barreteau, H., Kovac, A., Boniface, A., Sova, M., Gobec, S., and Blanot, D. (2008) Cytoplasmic steps of peptidoglycan biosynthesis. *FEMS Microbiol. Rev. 32*, 168–207.
7. Regni, C., Schramm, A. M., and Beamer, L. J. (2006) The reaction of phosphohexomutase from *Pseudomonas aeruginosa*: Structural insights into a simple processive enzyme. *J. Biol. Chem. 281*, 15564–15571.
8. Ray, W. J., Jr., and Long, J. W. (1976) Thermodynamics and mechanism of the PO_3^- transfer process in the phosphoglucomutase reaction. *Biochemistry 15*, 3993–4006.
9. Naught, L. E., and Tipton, P. A. (2001) Kinetic mechanism and pH dependence of the kinetic parameters of *Pseudomonas aerugi-*

nosa phosphomannomutase/phosphoglucomutase. *Arch. Biochem. Biophys. 396*, 111–118.
10. Zhang., G., Dai, J., Wang, L., Dunaway-Mariano, D., Tremblay, L. W., and Allen, K. N. (2005) Catalytic Cycling in β-Phosphoglucomutase: A Kinetic and Structural Analysis. *Biochemistry 44*, 9404–9416.
11. Rigden, D. J. (2008) The histidine phosphatase superfamily: Structure and function. *Biochem. J. 409*, 333–348.
12. Galperin, M. Y., Bairoch, A., and Koonin, E. V. (1998) A superfamily of metalloenzymes unifies phosphopentomutase and cofactor-independent phosphoglycerate mutase with alkaline phosphatases and sulfatases. *Protein Sci. 7*, 1829–1835.
13. Burroughs, A. M., Allen, K. N., Dunaway-Mariano, D., and Aravind, L. (2006) Evolutionary genomics of the HAD superfamily: Understanding the structural adaptations and catalytic diversity in a superfamily of phosphoesterases and allied enzymes. *J. Mol. Biol. 361*, 1003–1034.
14. Shackelford, G. S., Regni, C. A., and Beamer, L. J. (2004) Evolutionary trace analysis of the α-D-phosphohexomutase superfamily. *Protein Sci. 13*, 2130–2138.
15. Dai, J., Wang, L., Allen, K. N., Radstrom, P., and Dunaway-Mariano, D. (2006) Conformational cycling in β-phosphoglucomutase catalysis: Reorientation of the β-D-glucose 1,6-(bis)phosphate intermediate. *Biochemistry 45*, 7818–7824.
16. Rhyu, G. I., Ray, W. J., Jr., and Markley, J. L. (1984) Enzyme bound intermediates in the conversion of glucose 1-phosphate to glucose 6-phosphate by phosphoglucomutase. Phosphorus NMR studies. *Biochemistry 23*, 252–260.
17. Naught, L. E., and Tipton, P. A. (2005) Formation and Reorientation of Glucose 1,6-Bisphosphate in the PMM/PGM Reaction: Transient-State Kinetic Studies. *Biochemistry 44*, 6831–6836.
18. Rigden, D. J., Lamani, E., Mello, L. V., Littlejohn, J. E., and Jedrzejas, M. J. (2003) Insights into the catalytic mechanism of cofactor-independent phosphoglycerate mutase from X-ray crystallography, simulated dynamics and molecular modeling. *J. Mol. Biol. 328*, 909–920.
19. Koonin, E. V., and Tatusov, R. L. (1994) Computer analysis of bacterial haloacid dehalogenases defines a large superfamily of hydrolases with diverse specificity. Application of an iterative approach to database search. *J. Mol. Biol. 244*, 125–132.
20. Allen, K. N., and Dunaway-Mariano, D. (2004) Phosphoryl Group Transfer: Evolution of a Catalytic Scaffold. *Trends Biochem. Sci. 29*, 495–503.
21. Wang, W., Cho, H. S., Kim, R., Jancarik, J., Yokota, H., Nguyen, H. H., Grigoriev, I. V., Wemmer, D. E., and Kim, S. H. (2002) Structural characterization of the reaction pathway in phosphoserine phosphatase: Crystallographic "snapshots" of intermediate states. *J. Mol. Biol. 319*, 421–431.
22. Ridder, I. S., Rozeboom, H. J., Kalk, K. H., and Dijkstra, B. W. (1999) Crystal structures of intermediates in the dehalogenation of haloalkanoates by L-2-haloacid dehalogenase. *J. Biol. Chem. 274*, 30672–30678.
23. Zhang, G., Dunaway-Mariano, D., Mazurkie, A. S., and Allen, K. N. (2002) Evidence for an Induced Fit Model of Phosphonatase Catalysis: Determination of the pKa of the Schiff Base Forming Lys53. *Biochemistry 41*, 13370–13377.
24. Lahiri, S. D., Zhang, G., Dai, J., Dunaway-Mariano, D., and Allen, K. N. (2004) Analysis of the substrate specificity loop of the HAD superfamily cap domain. *Biochemistry 43*, 2812–2820.
25. Lahiri, S. D., Zhang, G., Dunaway-Mariano, D., and Allen, K. N. (2003) The Pentacovalent Phosphorus Intermediate of a Phosphoryl Transfer Reaction. *Science 229*, 2067–2071.
26. Bond, C. S., White, M. F., and Hunter, W. N. (2002) Mechanistic implications for *Escherichia coli* cofactor-dependent phosphoglycerate mutase based on the high-resolution crystal structure of a vanadate complex. *J. Mol. Biol. 316*, 1071–1081.
27. Lahiri, S. D., Zhang, G., Radstrom, P., et al. (2002) Crystallization and preliminary X-ray diffraction studies of α-phosphoglucomutase from *Lactococcus lactis*. *Acta Crystallogr. D58*, 324–326.
28. Qian, N., Stanley, G. A., Hahn-Hagerdal, B., and Radstrom, P. (1994) Purification and characterization of two phosphoglucomutases from *Lactococcus lactis* subsp. *lactis* and their regulation in maltose- and glucose-utilizing cells. *J. Bacteriol. 176*, 5304–5311.
29. Otwinowski, Z., and Minor, W. (1997) Processing of X-ray Diffraction Data Collected in Oscillation Mode. *Methods Enzymol. 276*, 307–326.
30. Collaborative Computational Project No. 4 (1994) The CCP4 suite: Programs for protein crystallography. *Acta Crystallogr. D50*, 760–763.
31. Adams, P. D., Grosse-Kunstleve, R. W., Hung, L. W., Ioerger, T. R., McCoy, A. J., Moriarty, N. W., Read, R. J., Sacchettini, J. C., Sauter, N. K., and Terwilliger, T. C. (2002) PHENIX:Building new software for automated crystallographic structure determination. *Acta Crystallogr. D58*, 1948–1954.
32. Emsley, P., and Cowtan, K. (2004) Coot: Model-building tools for molecular graphics. *Acta Crystallogr. D60*, 2126–2132.
33. Davis, I. W., Murray, L. W., Richardson, J. S., and Richardson, D. C. (2004) MOLPROBITY: Structure validation and all-atom contact analysis for nucleic acids and their complexes. *Nucleic Acids Res. 32*, W615–W619.
34. Lu, Z., Dunaway-Mariano, D., and Allen, K. N. (2008) The Catalytic Scaffold of the HAD Enzyme Superfamily Acts as a Mold for the Trigonal Bipyramidal Transition State. *Proc. Natl. Acad. Sci. U.S.A. 105*, 5687–5692.
35. Hayward, S., and Berendsen, H. J. C. (1998) Systematic Analysis of Domain Motions in Proteins from Conformational Change: New Results on Citrate Synthase and T4 Lysozyme. *Proteins: Struct., Funct., Genet. 30*, 144–154.

BI801653R